

# Manifestation of ground state anomaly in the core level spectra of Ca and Sr in $\text{Ca}_{1-x}\text{Sr}_x\text{RuO}_3$

Ravi Shankar Singh and Kalobaran Maiti

*Department of Condensed Matter Physics and Materials Science,*

*Tata Institute of Fundamental Research, Homi Bhabha Road, Colaba, Mumbai - 400005, INDIA*

(Dated: March 23, 2022)

We investigate the evolution of Ca  $2p$  and Sr  $3d$  core level spectra in  $\text{Ca}_{1-x}\text{Sr}_x\text{RuO}_3$  using photoemission spectroscopy. Core level spectra in this system exhibit multiple features and unusual evolution with the composition and temperatures. Analysis of the core level spectra in conjunction with the band structure results reveal novel final state effects due to different core hole screening channels. Changes in the core level spectra suggest significant modification in Ca-O covalency in Ca dominated samples, which gradually reduces with the increase in Sr content and becomes minimum in  $\text{SrRuO}_3$ . This study thus, provides a direct evidence of the role of cation-oxygen covalency in the ground state properties of these novel materials.

PACS numbers: 71.27.+a, 71.70.Fk, 79.60.Bm

Ruthenates have drawn significant attention in the recent time due to many interesting properties such as superconductivity [1], non-Fermi liquid behavior [2, 3], unusual magnetic ground states [2, 3, 4, 5] *etc.* observed in these materials.  $\text{SrRuO}_3$ , a perovskite compound exhibits ferromagnetic long range order ( $T_C = 160$  K) despite highly extended  $4d$  character of the valence electrons [4, 5]. Interestingly,  $\text{CaRuO}_3$ , an isostructural compound exhibit similar magnetic moment at high temperatures as that observed in  $\text{SrRuO}_3$ , however, no long-range order is observed down to the lowest temperature studied [2, 3, 4, 5]. These investigations predict a non-Fermi liquid ground state in  $\text{CaRuO}_3$  in contrast to the Fermi-liquid behavior observed in  $\text{SrRuO}_3$  [2, 3]. Both  $\text{SrRuO}_3$  and  $\text{CaRuO}_3$  form in an orthorhombic perovskite structure ( $\text{ABO}_3$  - type) [6, 7]. It is believed that the A cation (Sr/Ca) sites help to form the typical building block of this structure and the  $\text{RuO}_6$  octahedra connected by corner sharing essentially determines the electronic properties. The Ru-O-Ru bond angles are somewhat different in these compounds ( $165^\circ$  in  $\text{SrRuO}_3$  and  $150^\circ$  in  $\text{CaRuO}_3$ ) suggesting an enhancement in effective electron correlation strength. However, a recent experimental study shows that such effects are significantly weak as expected for a highly extended  $4d$  transition metal oxides [8] and thus, the experimental observation of different ground state properties still remains a puzzle.

Photoemission spectroscopy has widely been used to study these systems. However, the electronic states corresponding to A-site cations have often been neglected due to the absence of significant contribution from these elements in the vicinity of the Fermi level. In this study, we investigate the evolution of the core level spectra associated to the A-site cations. High quality polycrystalline samples (large grain size achieved by long sintering at the preparation temperature) were prepared by solid state reaction method using ultra-high purity ingredients and characterized by  $x$ -ray diffraction (XRD)

patterns and magnetic measurements as described elsewhere [4, 8]. Sharp XRD patterns reveal pure  $\text{GdFeO}_3$  structure with similar lattice constants as observed for single crystalline samples [5]. Photoemission measurements were performed on *in situ* ( $4 \times 10^{-11}$  torr) scraped samples using SES2002 Scienta analyzer. Reproducibility and cleanliness of the sample surface was confirmed after each trial of scraping.

In Fig. 1, we show Ca  $2p$  and Sr  $3d$  core level spectra for  $x = 0.0, 0.2, 0.5, 0.7$  and  $1.0$  in  $\text{Ca}_{1-x}\text{Sr}_x\text{RuO}_3$ . All the spectra are normalized by integrated intensity and exhibit multiple features in contrast to the spin orbit split two peak structure expected. This is unusual as  $\text{Ca}^{2+}$  and  $\text{Sr}^{2+}$  are believed to be highly ionic in nature with the unoccupied  $d$  bands appearing significantly above the Fermi level. There are four distinct features marked by A, B, C and D in all the Ca  $2p$  spectra shown in the left column of the figure. Despite large spin orbit splitting ( $\sim 3.5$  eV) for the Ca  $2p$  signals, experiments on several sets of samples in different experimental setups and high energy resolution (300 meV) do not exhibit any significant difference in the spectral features. A reduction in excitation energy (from Al  $K\alpha$  (open circles) to Mg  $K\alpha$  (triangles)) leads to a small increase in intensity of the features B and D. Since such a change in photon energy increases the surface sensitivity of the technique due to the reduction of the photoelectron kinetic energies, such spectral modification is often considered as the signature to identify the bulk and surface related features [9, 10]. However, several intriguing effects observed on variation of different parameters as described below, cannot be explained within this scenario.

We show the Al  $K\alpha$  spectra at 20 K by solid circles in the same figure. While features A and C remains at the same energies, a shift of the features B and D to lower binding energies is clearly evident as shown by B' and D' in the figure. This reveals that the changes in the features A and C separated by about 3.5 eV are very similar, and

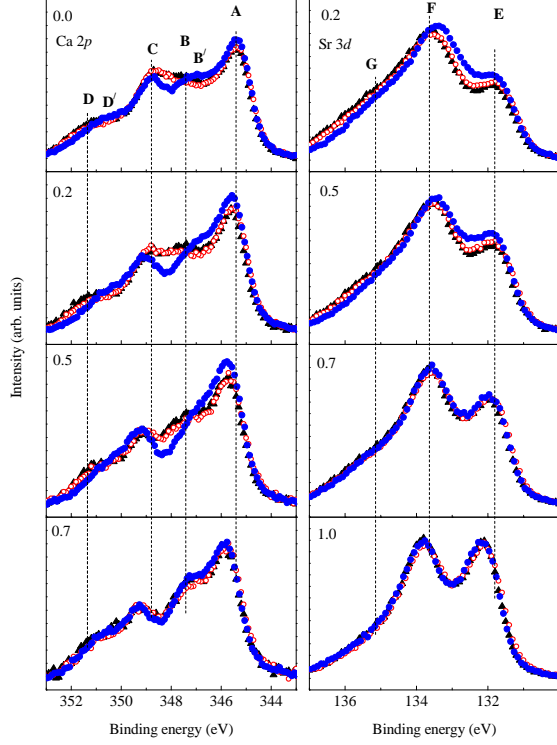


FIG. 1: Ca  $2p$  (left column) and Sr  $3d$  (right column) core level spectra in  $\text{Ca}_{1-x}\text{Sr}_x\text{RuO}_3$  for different values of  $x$ . Triangles, open circles and solid circles represent the spectra collected using Mg  $K\alpha$  radiations at 300 K, Al  $K\alpha$  radiations at 300 K and Al  $K\alpha$  radiations at 20 K, respectively.

the features B and D are connected together with an energy separation of about 3.5 eV. Thus, the features A and B ( $B'$ ) can be attributed to the photoemission signal due to the excitation of Ca  $2p_{3/2}$  electrons, and the features C, D ( $D'$ ) appear due to  $2p_{1/2}$  electronic excitations. The spectral modifications are found to be significantly large in  $\text{CaRuO}_3$ . Interestingly, the peak position of the features A and C gradually shifts to higher binding energies with the increase in  $x$ , while the features B and D appears almost at same binding energies across the series. In addition, the spectral modification with temperature gradually becomes insignificant with the increase in  $x$ .

We now turn to the Sr  $3d$  core level spectra. Although, a distinct set of spin orbit split  $3d$  signal is visible in the Sr  $3d$  spectra of  $\text{SrRuO}_3$  ( $x = 1.0$ ), the ratio of the intensity of  $3d_{5/2}$  and  $3d_{3/2}$  does not follow the expected multiplicity ratio of 3:2. All the spectra in the intermediate compositions exhibit three distinct features as shown by E, F and G in the figure. Most interestingly, the feature F appearing at about 133.6 eV binding energy exhibit the largest intensity, in sharp contrast to the expectation of lower intensity corresponding to the spin orbit split  $3d_{3/2}$  signal compared to the  $3d_{5/2}$  signal, E appearing at about 131.8 eV. The change in photon en-

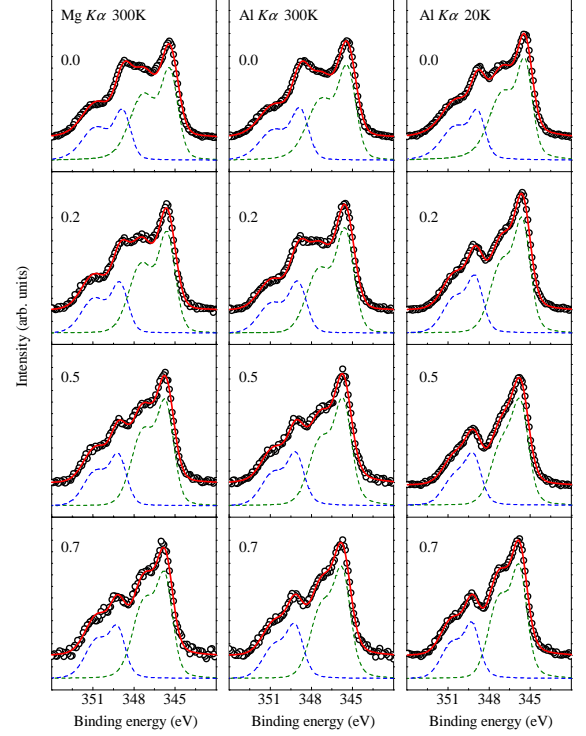


FIG. 2: Experimental (circles) and simulated (solid lines) Ca  $2p$  spectra for different  $x$  in  $\text{Ca}_{1-x}\text{Sr}_x\text{RuO}_3$ . The dashed lines represent the  $2p_{3/2}$  and  $2p_{1/2}$  features delineated from the experimental spectra.

ergy from Al  $K\alpha$  to Mg  $K\alpha$  does not exhibit significant modifications in the spectral features. However, the decrease in temperature leads to a shift of the feature F towards lower binding energies in  $\text{Ca}_{0.8}\text{Sr}_{0.2}\text{RuO}_3$ . With the increase in  $x$ , this shift becomes gradually insignificant as also observed in Ca  $2p$  spectra. The feature E shifts towards higher binding energies with the increase in  $x$ . Interestingly, the change in photon energy and temperature has no influence in the Sr  $3d$  spectra in  $\text{SrRuO}_3$ .

In order to investigate the spectral changes in more detail, we have simulated all the core level spectra using two sets of Lorentzians (representing lifetime broadening of the photoholes), where each set represents a spin orbit split two signals. These Lorentzians are convoluted with a Gaussian to consider resolution broadening and other solid state effects. In order to reduce the uncertainty in the fitting procedure, we have fixed the spin-orbit splitting to 3.47 eV for Ca  $2p$  and 1.7 eV for Sr  $3d$  spectra found in  $\text{CaRuO}_3$  and  $\text{SrRuO}_3$ , respectively. The fits are carried out using least square error method by varying the energy separation and the relative intensity of two sets of features.

The simulated spectra for all the Ca  $2p$  spectra are shown by solid lines in Fig. 2 by overlapping over the experimental spectra. All the fits exhibit a beautiful repre-

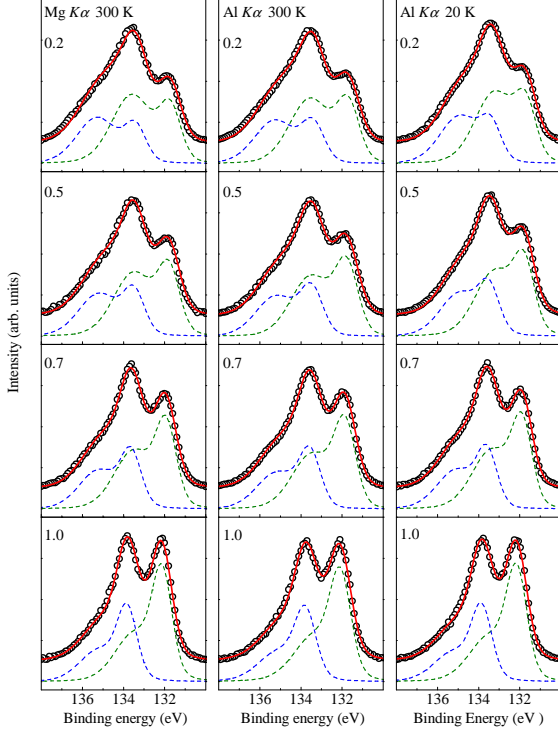


FIG. 3: Experimental (circles) and simulated (solid lines) Sr 3d spectra for different  $x$  in  $\text{Ca}_{1-x}\text{Sr}_x\text{RuO}_3$ . The dashed lines represent the  $3d_{5/2}$  and  $3d_{3/2}$  features delineated from the experimental spectra.

sensation of the experimental spectra. Clearly,  $2p_{3/2}$  and  $2p_{1/2}$  features contains at least two features in each case. The energy separation between the features in  $\text{CaRuO}_3$  is found (error bar = 0.02 eV) to be 1.9 eV, which reduces to 1.6 eV at 20 K. The energy separation gradually reduces with the increase in  $x$  (1.88 eV, 1.65 eV and 1.5 eV for  $x = 0.2, 0.5$  and  $0.7$ , respectively). However, the low temperature spectra do not exhibit such large change (1.5 eV, 1.4 eV and 1.45 eV for  $x = 0.2, 0.5$  and  $0.7$ , respectively). The most notable point is that the difference between room temperature and low temperature spectra gradually reduces with the increase in  $x$ . The simulated Sr 3d spectra are shown by solid lines overlapped over the experimental ones in Fig. 3. Anomalous high intensity observed for the feature F in the experimental spectra (see Fig. 1) could be simulated exactly considering two peak structure for the photoemission signal corresponding to each spin-orbit split features. The intensity of the higher binding energy feature is found to be significantly high compared to other one in the Ca-dominated compositions. This intensity reduces drastically with the increase in Sr-content across the series. The energy separation between the two features is found to be 1.85 eV at room temperature for  $x = 0.2$ . With the increase in  $x$  this separation reduces gradually (1.7 eV, 1.6 eV and

1.3 eV for  $x = 0.5, 0.7$  and  $1.0$ , respectively). The reduction in temperature leads to a decrease in the separation of the two features to 1.5 eV, 1.4 eV, 1.4 eV and 1.3 eV for  $x = 0.5, 0.7$  and  $1.0$ , respectively. Thus, the influence of temperature on the energy separation between the two features in each spin-orbit split signal gradually reduces with the increase in Sr-content and becomes invisible in  $\text{SrRuO}_3$ .

It is now clear that the two peak structure in the Ca  $2p$  and Sr  $3d$  core level spectra cannot be attributed to the differences in Madelung potential at A-sites present in the structure and/or surface-bulk related differences. In particular, various structural analysis also suggest that all the A-site cations are equivalent even if the structure is significantly distorted from the cubic perovskite structure. It is to note here that various binary and ternary compounds involving rare-earths at the A-site often exhibit additional features in the core level spectra. For example, La  $3d$  spectra in  $\text{La}_2\text{O}_3$ ,  $\text{LaM}_3$  ( $M$  is a monovalent element such as F, Br, Pd *etc.* [11, 12, 13]) exhibit distinct two peaks due to different screening channels in the photoemission final states. Thus, the two peak structures in the Ca  $2p$  and Sr  $3d$  core level spectra in these compounds can be attributed to differently screened final states.

The ground state wave function can be expressed as a linear combination of electronic states having different  $d$ -band occupancy such as  $|d^0\rangle$ ,  $|d^1L\rangle$  *etc.*, where  $L$  represents a hole in the oxygen band. The  $d$  bands corresponding to Ca ( $3d$ ) and Sr ( $4d$ ) are almost empty and appear significantly above the Fermi level ( $> 4$  eV). Thus, the charge transfer energy, the energy required to transfer an electron from the O  $2p$  bands to the  $d$ -bands is expected to be significantly high. Therefore, the contributions from the charge transferred states ( $|d^1L\rangle$ ,  $|d^2L^2\rangle$  *etc.*) will be energetically less favorable and the initial state will be primarily contributed by  $|d^0\rangle$  electronic configuration. In the final state, core holes created by the photoemission enhance the local positive charge density. Hence, the core holes are often screened by the electrons transferred from the ligand bands and are energetically most favorable. The photoemission signals corresponding to these final states are known as *well screened* or *main* peak and appear at lower binding energies. The feature corresponding to the core holes without any screening by such charge transfer are known as *poorly screened* or *satellite* features. The energy separation and the relative intensity of the main and satellite features depend on the charge transfer energy and the O  $2p$  - A-site  $d$  hybridization. It is to note here that if this hybridization is zero, the well screened feature will be insignificant.

In order to investigate the Ca-O and Sr-O hybridization, we have calculated the electronic band structure of this system using full potential linearized augmented plane wave method within the local spin density approxi-

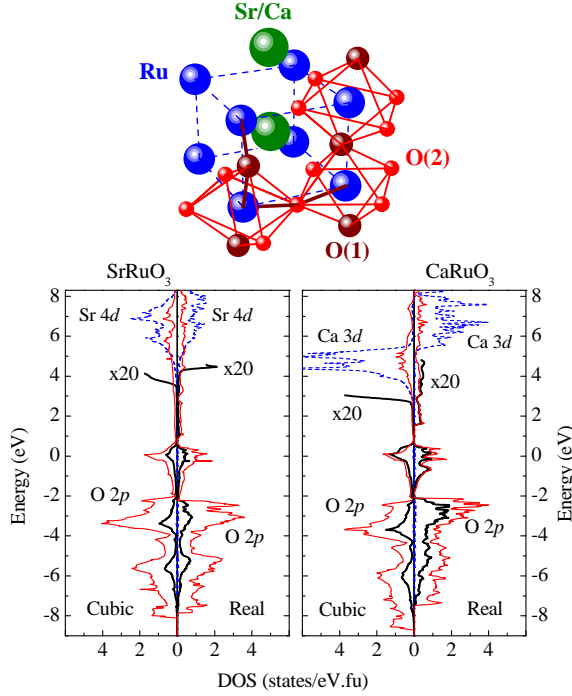


FIG. 4: Crystal structure of  $\text{SrRuO}_3$  and  $\text{CaRuO}_3$ . Band structure results for  $\text{SrRuO}_3$  and  $\text{CaRuO}_3$  in the real and equivalent cubic structures are shown in lower left and right panels, respectively. O  $2p$  and Sr  $4d$ /Ca  $3d$  PDOS are represented by thin solid lines and dashed lines, respectively. The thick solid line represent the Sr  $4d$ /Ca  $3d$  PDOS multiplied by 20 to amplify the low energy part.

mations (WIEN2K software[14]). The calculated results for Sr  $4d$  and O  $2p$  partial density of states (PDOS) in the real crystal structure and in the equivalent cubic structure (unit cell volume kept fixed) of  $\text{SrRuO}_3$  are shown in the left panel of Fig. 4. Sr  $4d$  contributions essentially appears above 3.6 eV in the cubic structure as shown by scaling the Sr  $4d$  PDOS by 20 times. A significant contribution from O  $2p$  PDOS appears in this energy range. Interestingly, the Sr  $4d$  band edge shifts to 4.4 eV in the real structure along with a significant modification in the O  $2p$  PDOS. Such changes indicate finite Sr-O covalency forming bonding and antibonding bands, which leads to a  $\text{GdFeO}_3$  kind of distortion by moving O(1) towards A-site as shown in Fig. 4.[15] The bonding band with primarily O  $2p$  character appears below the Fermi level and the antibonding band having primarily Sr  $4d$  character appears above the Fermi level. The calculated results in  $\text{CaRuO}_3$  are shown in the right panel of Fig. 4. The Ca  $3d$  PDOS exhibit the lower energy edge with significant intensity at 2.6 eV as expected for  $3d$  orbitals compared to  $4d$  orbitals in  $\text{SrRuO}_3$ . Most strikingly, the  $3d$  band shifts to much higher energies (band edge at 5.5 eV) com-

pared to that observed in the  $4d$  band in  $\text{SrRuO}_3$ . Such a strong modification is unusual and clearly reveal strong Ca-O covalency effects due to the large overlap of the O  $2p$  and Ca  $3d$  bands similar to that in vanadates [16].

These results establish that the hybridization of the  $d$  bands associated to A-site elements with O  $2p$  bands is significant. The higher energy of the Ca  $3d$  band compared to Sr  $4d$  conduction band suggests that the charge transfer energy for the electrons from O  $2p$  bands to A-site  $d$  bands is significantly larger in  $\text{CaRuO}_3$  than that in  $\text{SrRuO}_3$ . This explains the observation of larger energy separation between the well screened and poorly screened features in the core level spectra, and the gradual reduction of this separation with the increase in Sr-content.

The  $\text{GdFeO}_3$  distortion observed in this system, reduces the Ru-O-Ru bond angles significantly from  $180^\circ$ . Subsequently, the  $\text{RuO}_6$  octahedra also becomes distorted leading to different O-O couplings. Thus, the O  $2p$  bandwidth reduces significantly as evident in the calculated results for real structure in comparison to that in the equivalent cubic structure. Such narrowing significantly affects the delocalization of holes created in the O  $2p$  band due to charge transfer. This is manifested by an increase in intensity of the poorly screened feature compared to the well screened feature intensity towards  $\text{CaRuO}_3$  end of  $\text{Ca}_{1-x}\text{Sr}_x\text{RuO}_3$  in both Ca  $2p$  and Sr  $3d$  spectra (see Figs. 2 and 3).

We now turn to the question of temperature evolution in the core level spectra. The peak position of the satellite feature shifts (0.3 eV in  $\text{CaRuO}_3$  and gradually reduces with increase in  $x$ ) to lower binding energies. This can qualitatively be explained as follows. It is now clear that the strong A-O covalency leads to a  $\text{GdFeO}_3$  distortion in the crystal structure [15, 16]. While large covalency increases the separation between the unoccupied  $d$  band (antibonding) and occupied O  $2p$  band (bonding), the center of mass of the bonding band is observed to shift towards the Fermi level (see Fig. 4). The decrease in temperature leads to a compression of the crystal lattice. While such compression leads to an enhancement in the bandwidth due to reduction in bond lengths (a reduction in charge transfer energy), it often introduces a larger degree of distortion as observed in the bulk properties due to application of external pressure on  $\text{SrRuO}_3$  [17]. Thus, the effective potential at the A-sites will be modified with the decrease in temperature leading to a reduction in binding energy of the poorly screened feature in addition to a decrease in the main peak-satellite separation due to the reduction in charge transfer energy. It is clear that the electronic structure in  $\text{CaRuO}_3$  is significantly influenced by the change in temperature, however, that in  $\text{SrRuO}_3$  is relatively insensitive. While it is natural to draw an interconnection of such temperature induced changes in electronic structure to the non Fermi liquid behavior in  $\text{CaRuO}_3$ , further studies are required to understand the temperature evolutions in great

detail.

In summary, we have investigated the evolution of the core level spectra associated to the A-site in  $\text{ABO}_3$  structure as a function temperature and composition in  $\text{Ca}_{1-x}\text{Sr}_x\text{RuO}_3$ . Photoemission results exhibit multiple structures in the core level spectra. Analysis of the spectra reveal strong influence of core hole screening in the final states, a novel effect associated to A-sites in the  $\text{ABO}_3$  structure not studied so far. Evolution of the core level spectra with temperature and composition suggest that the distortion in the crystal structure and its change with temperature possibly play the key role in determining significantly different ground state properties in these interesting materials.

- 
- [1] Y. Maeno *et al.* Nature **372**, 532 (1994).
  - [2] P. Khalifah, I. Ohkubo, H. Christen, D. Mandrus, Phys. Rev. B **70**, 134426 (2004); Y. S. Lee, Jaejun Yu, J. S. Lee, T. W. Noh, T.-H. Gimm, Han-Yong Choi, C. B. Eom, Phys. Rev. B **66**, 041104(R) (2002).
  - [3] L. Klein, L. Antognazza, T.H. Geballe, M.R. Beasley, A. Kapitulnik, Phys. Rev. B **60**, 1448 (1999).
  - [4] R.S. Singh, P.L. Paulose, and K. Maiti, Solid State Physics: Proceedings of the DAE Solid State Physics symposium, **49**, 876 (2004).
  - [5] G. Cao, S. McCall, M. Shepard, J.E. Crow, R.P. Guertin, Phys. Rev. B **56**, 321 (1997).
  - [6] M.V. Rama Rao, V.G. Sathe, D. Sornadurai, B. Panigrahi, T. Shripathi, J. Phys. Chem. Solids, **62**, 797 (2001).
  - [7] H. Nakatsugawa, E. Iguchi, Y. Oohara, J. Phys.: Condens. Mater, **14**, 415 (2002).
  - [8] K. Maiti R.S. Singh, Phys. Rev. B **71**, 161102(R) (2005).
  - [9] K. Maiti *et al.*, Europhys. Lett. **55**, 246 (2001).
  - [10] K. Maiti *et al.*, Phys. Rev. B **73**, 052508 (2006).
  - [11] F.U. Hillebrecht J.C. Fuggle, Phys. Rev. B **25**, 3550 (1982).
  - [12] G. Crecelius, G.K. Wertheim, D.N.E. Buchanan, Phys. Rev. B **18**, 6519 (1978).
  - [13] A.J. Signorelli R.G. Hayes, Phys. Rev. B **8**, 81 (1973).
  - [14] P. Blaha, K. Schwarz, G.K.H. Madsen, D. Kvasnicka, J. Luitz, **WIEN2k**, An Augmented Plane Wave + Local Orbitals Program for Calculating Crystal Properties (Karlheinz Schwarz, Techn. Universität Wien, Austria) (2001) (ISBN 3-9501031-1-2).
  - [15] K. Maiti, Phys. Rev. B (2006) (appearing).
  - [16] E. Pavarini, S. Biermann, A. Poteryaev, A. I. Lichtenstein, A. Georges, O. K. Andersen, Phys. Rev. Lett. **92**, 176403 (2004).
  - [17] J.J. Neumeier, A.L. Cornelius, J.S. Schiling, Physica B **198**, 324 (1994).